Journal of Constructional Steel Research 147 (2018) 277–292

Contents lists available at ScienceDirect

Journal of Constructional Steel Research

Structural behavior of cold-formed thick-walled rectangular steel columns

Ziao Liu [b], Hongbo Liu [a,b,c,*], Zhihua Chen [a,b,c], Guoping Zhang [b]

[a] State Key Laboratory of Hydraulic Engineering Simulation and Safety, Tianjin University, Tianjin 300072, China
[b] Department of Civil Engineering, Tianjin University, Tianjin 300072, China
[c] Key Laboratory of Coast Civil Structure Safety of China Ministry of Education, Tianjin University, Tianjin 300072, China

ARTICLE INFO

Article history:
Received 12 November 2017
Received in revised form 24 February 2018
Accepted 17 March 2018
Available online xxxx

Keywords:
Cold-formed rectangular steel columns
Thick-walled
Axial load test
Numerical analysis
Design method

ABSTRACT

Cold-formed rectangular steel columns with large and thick walls are increasingly applied in engineering recently. The section dimension and wall thickness have increased continuously to 800 and 22 mm, respectively, which causes the significant differences of cold-formed effects between cold-formed rectangular steel columns with thin and thick walls. Therefore, the mechanical performance and design method of cold-formed rectangular steel columns with thick walls should be studied. In this study, two section dimensions (700 mm × 20 mm and 600 mm × 16 mm) were selected for the axial load test and analysis of cold-formed rectangular steel columns with large and thick walls. The conclusions are as follows. (1) The indirect cold-formed rectangular steel columns have lower cold-formed effects than direct cold-formed rectangular steel columns. (2) Cold-formed rectangular steel columns with large and thick walls have high-bearing capacity under axial loads, which are manifested by local plate instability. (3) Calculation formula of ultimate bearing capacity with considerations to local plate buckling is proposed. The calculated and test results are in accordance with numerical simulation results.

1. Introduction

Cold-formed steel is an efficient, economic, and environment-friendly building material with a reasonable section shape, good mechanical properties, and high steel utilization. Cold-formed steel possesses promising application prospects in the modern construction industry [1]. Currently, considerable research has mainly focused on cold-formed steel columns with thin walls. Relative systematic standards and guidelines for cold-formed steel columns with thin walls are issued [2–7]. The demands for cold-formed steel columns with thick walls have increased gradually with the development of cold-formed technology and large engineering construction. With the development of cold-formed steels, the height and thickness of cross-section of cold-formed thin-walled rectangular steel columns has reached 800 mm and 22 mm respectively, which have been used in the Tianjin Wanhui Square Project in China (Figs. 1–2). However, few studies have referred to the mechanical properties and the design method of large-section cold-formed steel columns with thick walls.

Wen conducted an experimental study on the axial bearing capacity of short cold-formed steel columns with wall thickness ranging 7.5–16 mm [8]. Li discussed the reliability of an axial compression member with 8–12 mm thick cold-formed steel columns [9–11]. Chen investigated the ultimate bearing capacity of cold-formed rectangular steel columns with 8–9 mm thick walls [12]. Liu examined the axial compression performance of cold-formed rectangular steel columns with 22 mm thick walls [13].

The previous research on cold-formed thin-walled and thick-walled section steel found that the cold hardening effect is intensified as the thickness increases; where the strength increases by 4% to 34% for thin-walled rectangular steel tube (0.4–6 mm thick) [14–16], but increases by 8% to 41% for thick-walled one (6–16 mm thick) [10,17–20]. For thin-walled cold-formed steel tube made by direct method, the yielding strength in the corner part is 30%–55% higher than that in the flat part, especially when the width-to-thickness ratio is large [10,14–16,19]; the strength of cold-formed member made by direct method is 6%–20% higher than that by indirect method [13,17].

Similar to rolled steel, the cold-formed steel also would experience different failure modes (overall buckling or local buckling) due to different slenderness ratio and width-to-thickness ratio [8,12,21,22], and the local buckling mainly occurred to the welding parts [19,11]. As

* Corresponding author at: State Key Laboratory of Hydraulic Engineering Simulation and Safety, Tianjin University, Tianjin 300072, China.
E-mail address: hbliu@tju.edu.cn (H. Liu).

https://doi.org/10.1016/j.jcsr.2018.03.013
0143-974X/

Fig. 1. Overview of Tianjin Wanhui Square Project.

Fig. 2. The construction site of Tianjin Wanhui Square Project.

the thickness grows, the material strength and the cold hardening effect increase, the yielding strength increases by 16%–41% compared to base metal [19,11].

The previous numerical studies for cold-form steel members was usually used FEM analysis, which considering the initial imperfection, material nonlinearity and geometric nonlinearity [5–7,13,14,23]; however, few research concerned about residual stress. The residual stress had some effect on the bearing capacity of cold-formed rectangular steel tube, for example the load bearing capacity would decrease by about 7% and the member would experience earlier failure [12,24–26].

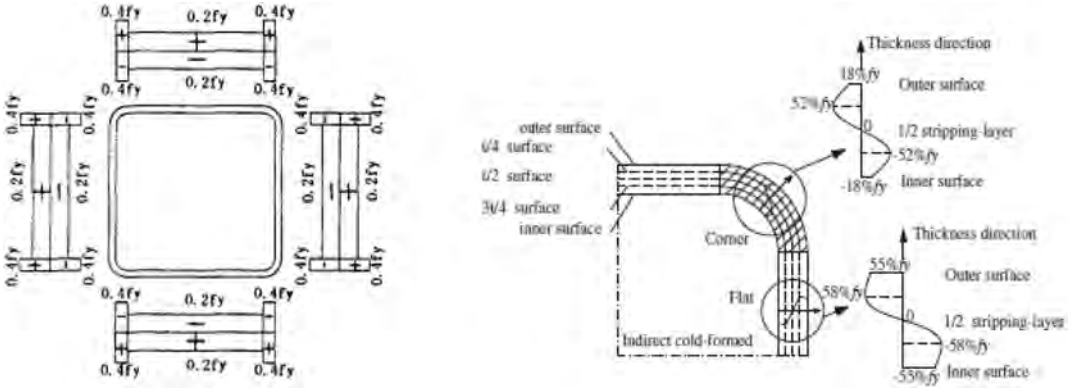

Fig. 3. Longitudinal distribution of residual stress for thin-walled cold-formed rectangular steel tube (0.4–6 mm).

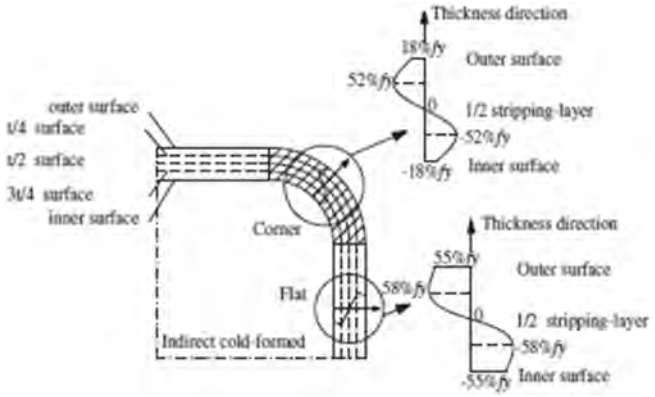

Fig. 4. Longitudinal distribution of residual stress for thick-walled cold-formed rectangular steel tube (10–16 mm).

The distribution and the amplitude of residual stress would vary with different thickness [17–19,27–30] (Figs. 3–5), leading to differences in mechanical performances; therefore, the thickness exerted obvious influence on the mechanical performances of cold-formed rectangular steel tube.

To sum up, insufficient research on mechanical properties and the design method of cold-formed steel columns with thick walls are found, which limited their engineering applications. In this paper, the axial compression performance and eccentric bearing capacity of indirect cold-formed rectangular steel columns with thick walls are investigated through test and numerical simulation. The calculation formula of axial loads and the eccentric bearing capacity of cold-formed rectangular steel columns with large sections and thick walls are proposed.

2. Test program

2.1. Specimen design

Cold-formed rectangular steel columns are divided into direct and indirect types according to forming processes [17,31]. A cold-formed square hollow section can be formed by rolling an annealed flat strip directly onto a square hollow section, which is then welded at the edges. A cold-formed hollow section can also be formed by first rolling an annealed flat strip onto a circular hollow section, which is then welded at the edges; the process is completed by further rolling onto a square hollow section. In this paper, the former forming process is called "direct square method", and the latter is called "indirect method from circular to square". In this study, indirect cold-formed rectangular steel columns are used as the specimen.

Considering the test cost and test equipment capability, two cold-formed rectangular steel column specimens are designed in this study (Fig. 6). The section dimension, thickness, and height of specimen 1 are 600 mm × 600 mm, 16 mm, and 2.4 m, respectively. The section dimension, thickness, and height of specimen 2 are 700 mm × 700 mm, 20 mm, and 2.4 m, respectively.

2.2. Mechanical properties of materials

Three standard tensile samples are cut and processed at the side and corner of each specimen. The static tensile test of 12 specimens is conducted to determine the basic mechanical properties of cold-formed rectangular steel columns. Fig. 7 depicts the sampling positions of specimens. All specimens are cut longitudinally. Fig. 8 illustrates the dimensions of specimens. The mean indexes of three specimens at the same position are used to determine the basic mechanical properties of materials. Given that several specimens have no evident yield platform, the yield strength is based on 0.2% of the residual strain. The material mechanics test data of 800 × 22 specimens refers to the method of Liu. Table 1 lists the elasticity modulus, yield strength, ultimate strength, yield ratio, and elongation of materials at different positions. Fig. 9 shows the stress–strain curve, and Fig. 10 presents the failure morphology of a specimen.

On the basis of the test results in Table 1 and Figs. 9–10, the conclusions are summarized as follows:

(1) Standard tensile specimens have experienced three stages: yield, necking down, and fracture. Given that the cold-formed technology reduces the ductility of steel materials to some extent, most specimens have no evident yield platform.

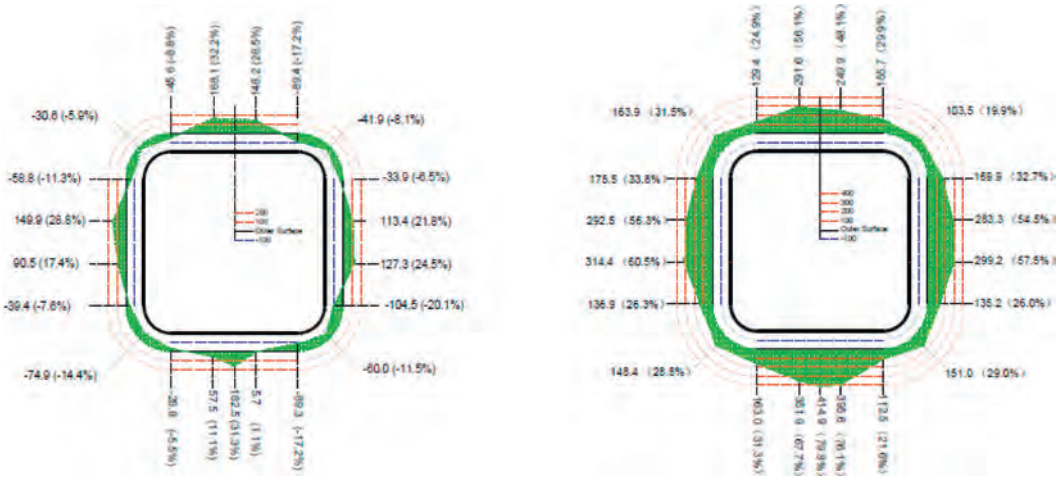

(a) Transverse cold-formed residual stress distribution on the external surface

(b) Longitudinal cold-formed residual stress distribution on the external surface

Fig. 5. Residual stress for cold-formed thick-walled rectangular steel tube (12 mm).

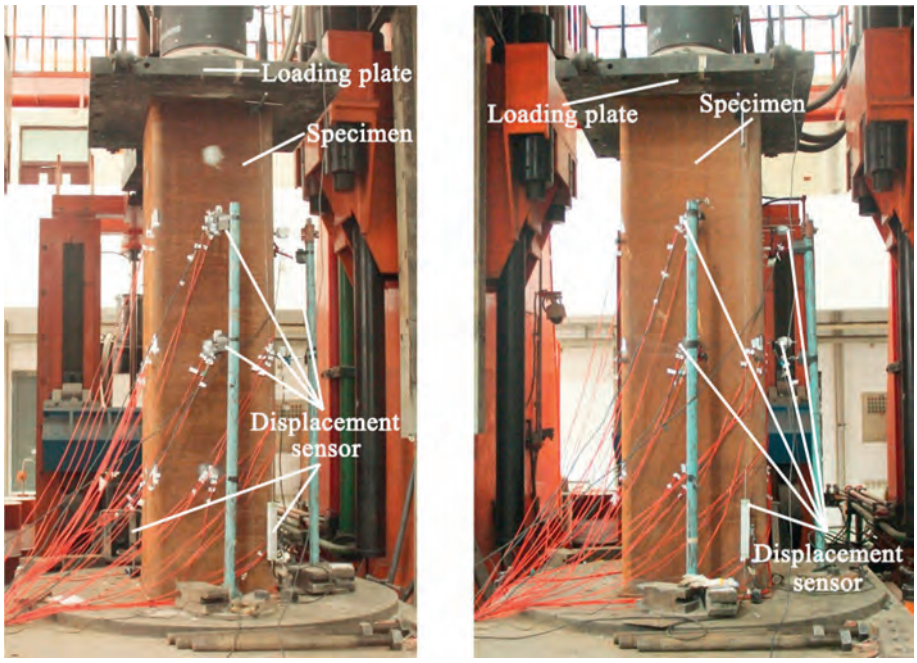

(a) Specimen 1: 600 mm×16 mm (b) Specimen 2: 700 mm×20 mm

Fig. 6. Specimen size.

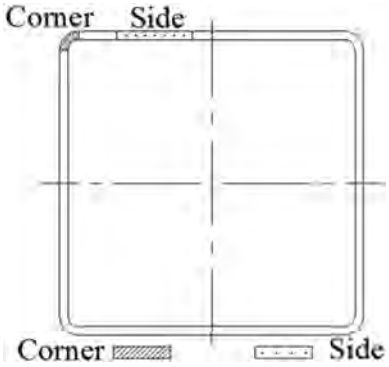

Fig. 7. Sampling positions of specimens.

(2) The yield strengths of the corner and side locations are significantly different. The yield strengths of the corner location are 18.57%, 16.18%, and 17.68% when the section dimensions are 600 mm × 16 mm, 700 mm × 20 mm, and 800 mm × 22 mm, respectively, which are higher than those in the side location. The difference of yield strength between the corner location and side location is reduced with the increase of the width-to-thickness ratio of the specimen.

(3) The cold-formed technique influences the material properties significantly. In other words, the cold-formed effect of the indirect cold-formed technique is lower than that of the direct cold-formed technique. For the thin-walled component manufactured by the direct cold-formed technique, the yield strength of the cor-

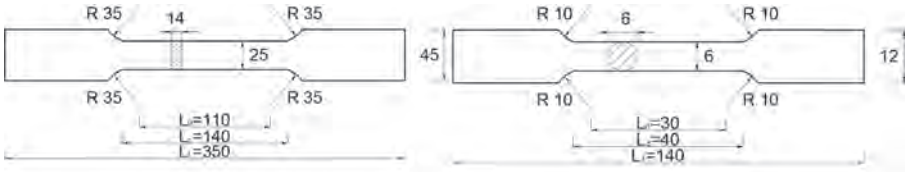

(a) Specimen at 600 side location; (b) Specimen at 600 corner location

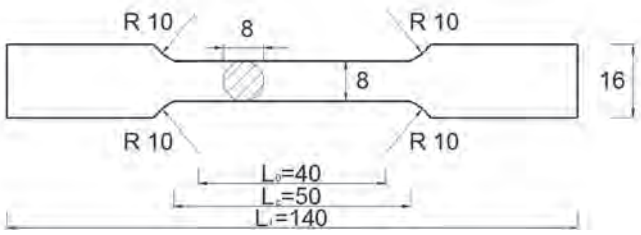

(c) Specimen at 700 side location and corner location

Fig. 8. Shape and dimension of specimens.

Table 1
Test results of material properties.

Dimension (mm)	Width-to-thickness ratio	Position	Yield strength (MPa)	Ultimate stregnth (MPa)	Young's modulus (GPa)	Yield ratio	Elongation
600 × 16	37.50	Side	350	450	209	0.778	27.70%
		Corner	415	499	206	0.832	14.00%
700 × 20	35.00	Side	340	443	214	0.767	28.10%
		Corner	395	488	208	0.809	17.60%
800 × 22	36.36	Side	328	434	213	0.756	30.00%
		Corner	386	472	211	0.818	25.20%

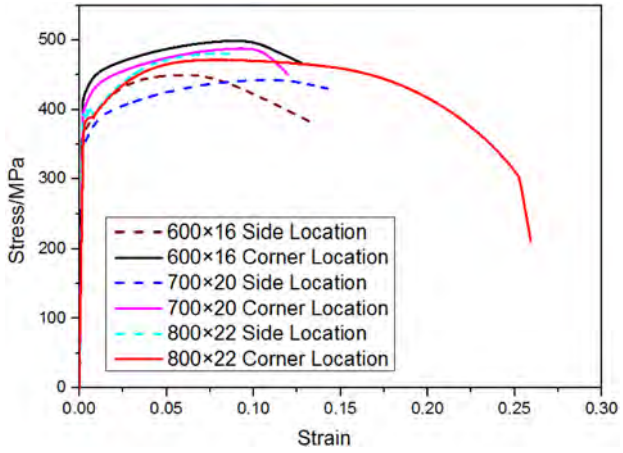

Fig. 9. Stress–strain curves.

ner location is 30–50% higher compared with the side location, which is significantly higher than component manufactured by the indirect cold-formed technique.

(4) A significant gap of ultimate strength is found between the corner location and the side location. The ultimate strengths of the corner location are 10.89%, 10.16%, and 8.76% when the section dimensions are 600 mm × 16 mm, 700 mm × 20 mm, and 800 mm × 22 mm, respectively, which are higher than those of the side locations. Such gap decreases with the increase of specimen thickness.

(5) The elongation of the cold-formed thick component is positively related to thickness. The elongation of the side location is higher than 20%, and the yield ratio is lower than 0.85. The elongation of the corner location is approximately 15%, and the yield ratio is roughly 0.9. The cold-formed thick component is highly sensitive to cold-formed effects.

According to the test data from Table 1, the mean yield strength of specimens can be calculated by Eq. (1). The yield strength of specimens is calculated according to the *Technical Code of Cold-formed Thin-wall Steel Structures* [32] Eq. (2), *North America/Australia/New Zealand Cold-formed Steel Structure* (AISI S100-2007) [33], (AS/NZS 4600-2005) [34] (Eq. (3)), and *European Design of Steel Structures* (EN 1993-1-6-2006) [35] (Eq. (4)). Table 2 lists the results.

$$f_1 = \frac{f_m A_m + f_c A_c}{A_e} \tag{1}$$

$$f_2 = \left[1 + \frac{\eta(12\gamma - 10t)}{l}\sum_{i=1}^{n}\frac{\theta_i}{2\pi}\right] f \tag{2}$$

$$f_3 = Cf_c + (1-C)f_m \tag{3}$$

$$f_4 = f_{yb} + \left(f_u - f_{yb}\right)\frac{knt^2}{A} \tag{4}$$

f_1 is the mean yield strength; f_m and f_c are the yield strength of flat location and corner location; A_m and A_c are the section area of the flat location and the corner location; A_e is the effective section; f_2 is the calculated strength according to *Technical Code of Cold-formed Thin-wall Steel Structures* [32]. f is the design strength before cold-formed process; η is the coefficient which depends on the forming process, in this study, the square columns are manufactured from circular columns, so $\eta = 1.7$; γ is the ratio of tensile strength to yield strength, regarding Q235 steel, $\gamma = 1.58$; t is the thickness of column section; l is the length of cross section central axial line; n is the number of corners of cross section, for the columns in this study $n = 4$; θ_i is the central angle of corner which is defined with rad; f_3 is the calculated strength according to AISI S100-2007 [33] or AS/NZS 4600-2005 [34]; $C = \frac{A_c}{A_m + A_c}$; f_4 is the calculated strength according to *European Design of Steel Structures* (EN 1993-1-6:2006) [35]; f_u and f_{yb} are the tensile strength and yield strength of the steel; A is the gross section area; k is the coefficient which depends on the shaping method, regarding cold rolled steel, $k = 7$.

Table 2 exhibits that the calculated results of different equations are close to the test values. The standard calculated results of different countries are relatively conservative. The average yield strength from Eq. (3) is 0.993 of measured yield strength, and the coefficient of variation is 0.008, which indicate that the calculated results are close to the test results. Therefore, the *North America/Australia/New Zealand*

(a) Side location (b) Corner location

Fig. 10. Fracture morphology of specimens.

Table 2
Comparison of calculated results of different standard formulas and test results.

Dimension	Test	GB 50018-2002		AISI S100-2007 AS/NZS 4600:2005		EN 1993-1-6:2006	
	f_1 (MPa)	f_2 (MPa)	f_2/f_1	f_3 (MPa)	f_3/f_1	f_4 (MPa)	f_4/f_1
600 × 16	357	302	0.846	352	0.984	310	0.868
700 × 20	345	294	0.853	343	0.995	305	0.884
800 × 22	333	291	0.875	333	1.000	305	0.917
Average value	345	296	0.858	343	0.993	307	0.890
Coefficient of variation	0.035	0.019	0.018	0.028	0.008	0.009	0.028

Design Specifications for Cold-formed Steel Structure [33,34] can be used in cold-formed rectangular steel columns with thick walls.

2.3. Loading scheme

Axial load was applied by electro-hydraulic servo oil press, and the diagonal vertical displacement of the plate section at the top column was measured by two displacement meters. The strains at key positions were tested by strain gauges. Strain gauges were installed at 1/4, 1/2, and 3/4 heights of the column (Fig. 11). Fig. 12 shows the overall test rig.

For a 700 × 700 × 20 specimen, 1600 kN (approximately 10% of the estimated ultimate load) is applied in advance. The loading process starts when all the components are contacted well and no transmission error of test signals is found. A stable loading is maintained during the loading process. First, the loading process is controlled by force and then controlled by displacement when the bearing capacity reaches roughly 13,000 kN. For a 600 × 600 × 16 specimen, 1100 kN (approximately 10% estimated ultimate load) is applied in advance. The loading process is controlled by force first and then controlled by displacement when the bearing capacity reaches roughly 10,000 kN. With the increase of displacement, the load decreases because it is used as the ultimate load.

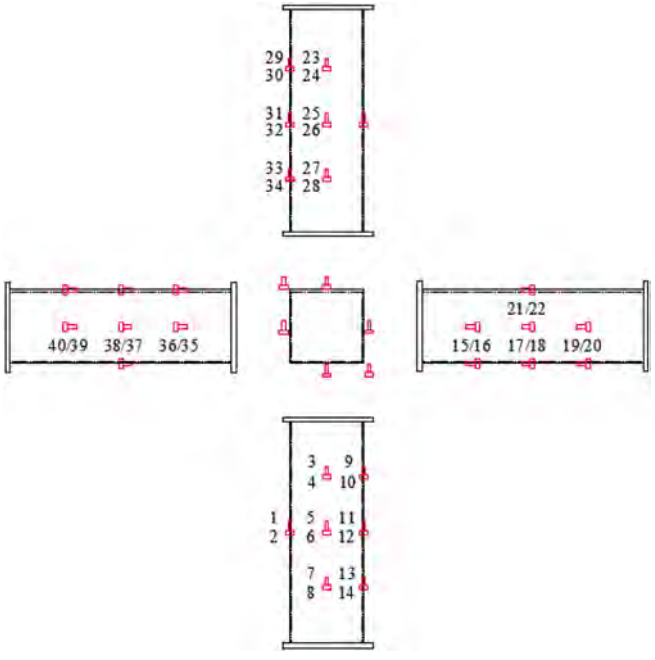

Fig. 11. Distribution of strain gauges.

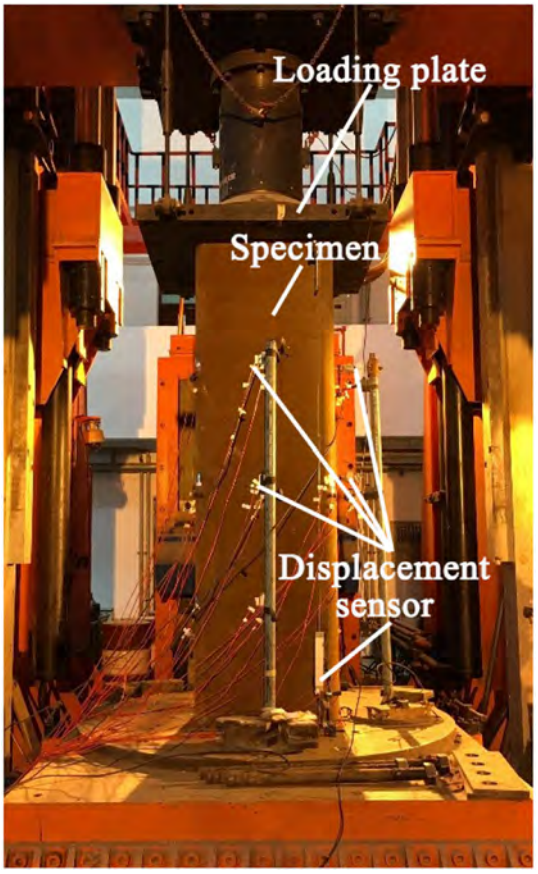

Fig. 12. Test apparatus for axial compression.

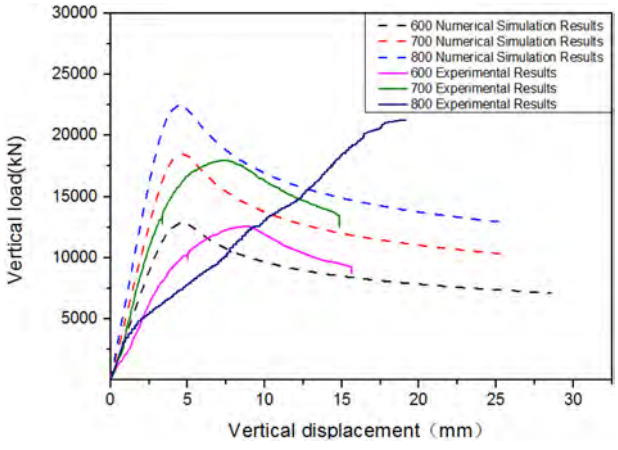

Fig. 13. Load–displacement curves.

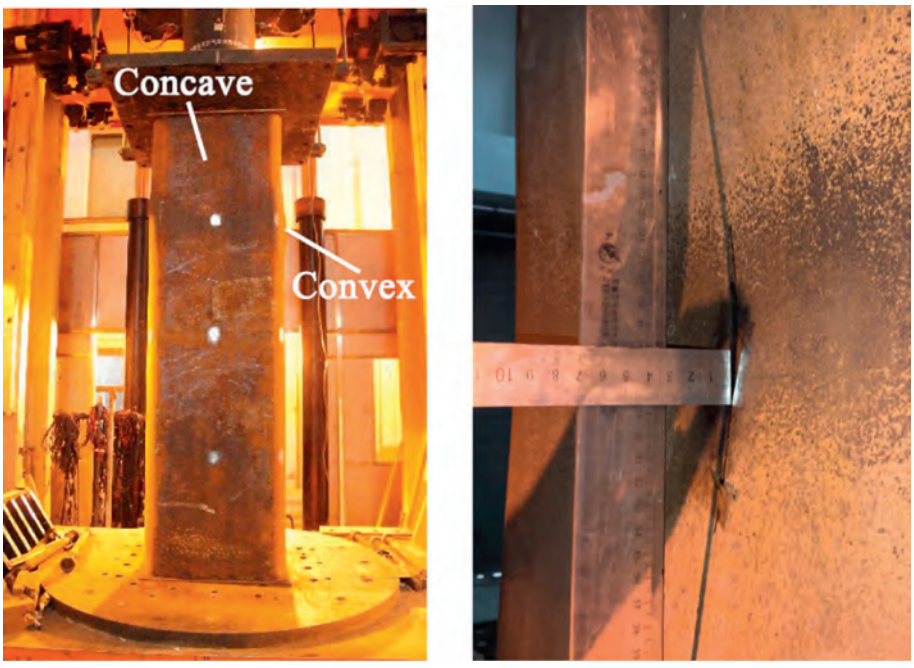

(a) 700×20 specimen (b) 700×20 concave surface

Fig. 14. Test failure of a 700 × 20 specimen.

3. Experimental result analysis

Ultimate loads of 700 × 20 and 600 × 16 specimens are 17,950 and 12,550 kN, respectively. Their maximum vertical deformations are 14.85 and 15.65 mm, respectively. Fig. 13 illustrates the load–displacement curves. According to the tested ultimate bearing capacity, the stability coefficients of specimens 1 and 2 are calculated (0.979 and 0.949). The 700 × 20 and 600 × 16 specimens presented local bump

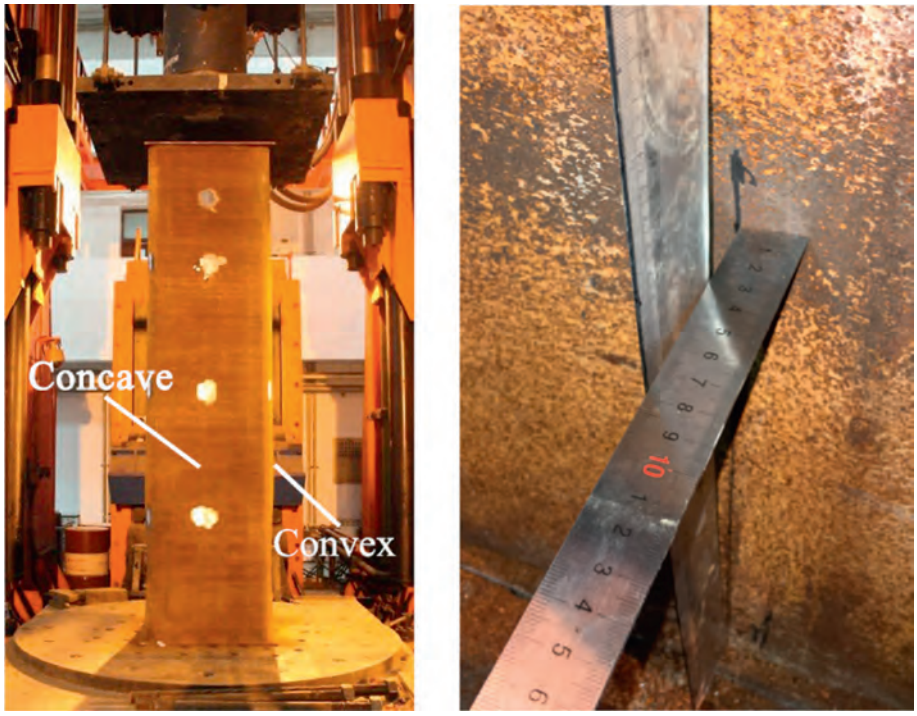

(a) 600×16 specimen (b) 600×16 concave surface

Fig. 15. Test failure of a 600 × 16 specimen.

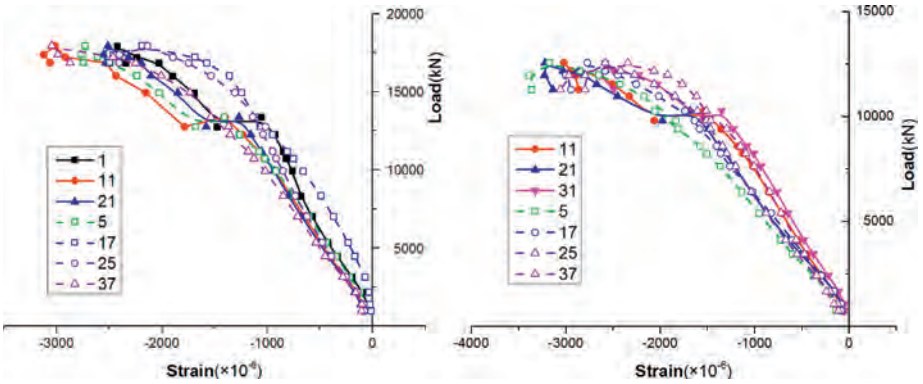

(a) 700×20 specimen (b) 600×16 specimen

Fig 16. Load–strain curves of middle section.

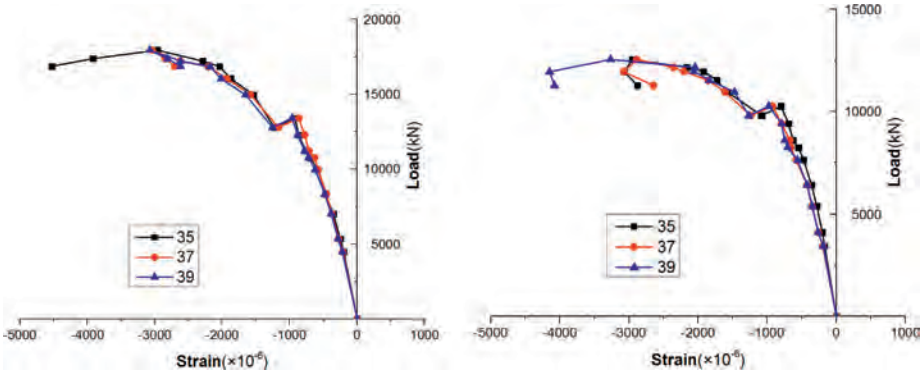

(a) 700×20 specimen (b) 600×16 specimen

Fig. 17. Load–strain curves of longitudinal direction.

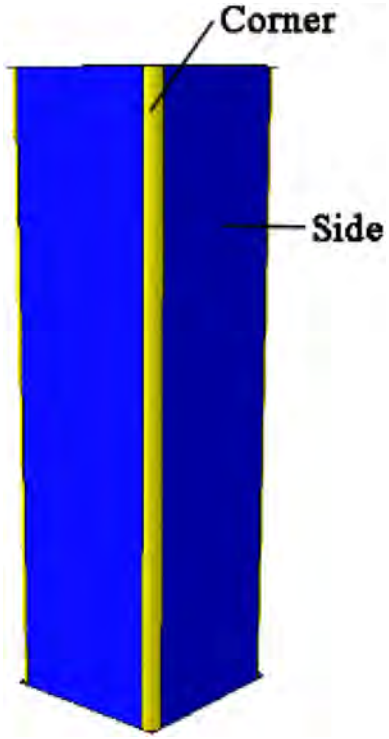

Fig. 18. Section division.

buckling deformation. Specifically, deformation is observed on the upper adjacent surface of a 700 × 20 specimen, and bump deformation is observed on the lower adjacent surface of a 600 × 16 specimen. Figs. 14 and 15 depict the failure modes.

Figs. 16 and 14 show the load–stress curves at key test points. Fig. 16 exhibits the load–strain curves at points 1, 11, 21, and 31 of the corner location and points 5, 17, 25, and 37. The sudden change of curves in Fig. 16 is caused by changing the loading mode. According to the observation points, the strain variations of the corner and side locations of two specimens are similar. Fig. 17 illustrates the load–strain curves at points 35, 37, and 39, which are distributed longitudinally on the convex surface. Point 35 of a 700 × 22 specimen and point 39 of a 600 × 16 specimen are the measuring points of the convex locations, in which the strain is significantly higher than the other measuring points of the convex surface.

4. Numerical simulation

Given the residual stress caused by the cold-formed process and cold-formed effect of materials, a finite element analysis model for cold-formed rectangular steel columns with thick walls was established. The results of the model were compared with the test data, which verified the feasibility of the model. The axial compression and eccentric compression performances of cold-formed rectangular steel columns

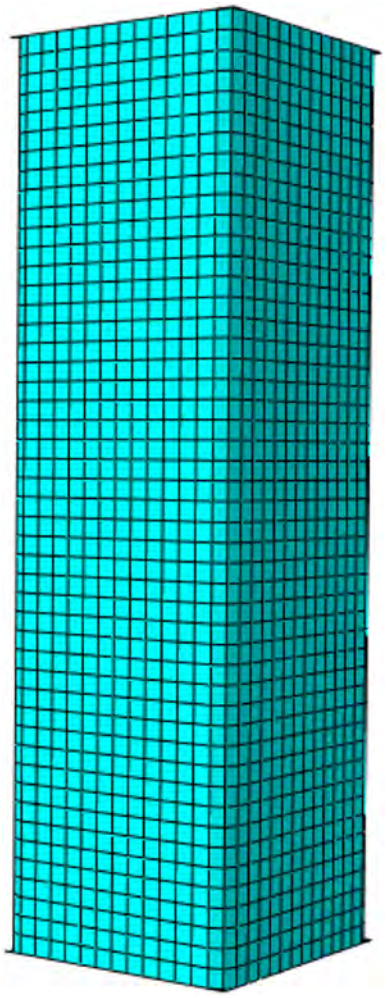

Fig. 19. Mesh.

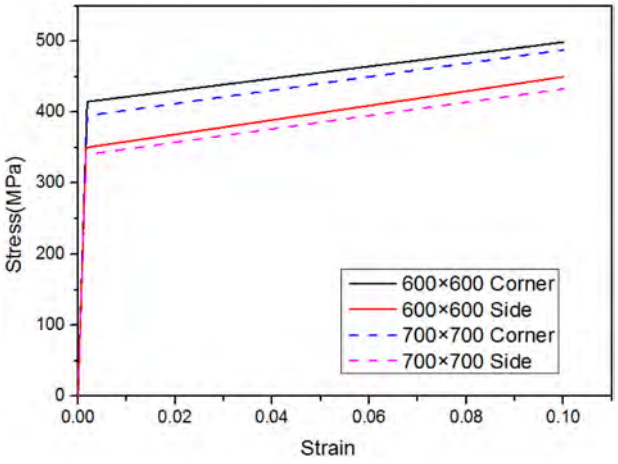

Fig. 20. Stress–strain curves in the finite element model.

with thick walls were discussed systematically by using the finite element model.

4.1. Simulation of axial compression behavior

The axial load bearing capacity of cold-formed rectangular steel columns with thick walls under the existence of initial imperfection and residual stress was analyzed by ABAQUS. This process is accomplished in three steps. Step 1: establish the finite element model. Step 2: introduce the residual stress for eigenvalues buckling analysis to obtain the worst initial imperfection distribution. Step 3: nonlinear analysis. One reference point is set at the top of the column and is coupled with the column by the consideration of material nonlinearity and geometric nonlinearity. Displacement is applied to this reference point, and the ultimate load is obtained.

According to material properties, the finite element model of cold-formed rectangular steel columns with thick walls is divided into two locations: corner and side locations (Figs. 18 and 19). Table 3 and Fig. 20 show the material properties of models.

The residual stress distribution model of cold-formed rectangular steel columns with thick walls, which was proposed by Zhang, was used to discuss the influences of residual stress on the mechanical properties of steel columns [18]. In this residual stress model, the internal and external surfaces are equal in size but opposite in signs (Fig. 21). Suppose that residual stress is present in the linear distribution along the thickness direction, f_y in Fig. 21 refers to yield strength at the corresponding position. The stress distribution of the 700 × 20 × 2400 stub column finite element analysis model after residual stress is introduced (Fig. 22). First, eigenvalue buckling was analyzed, which obtained the critical buckling load of elastoplasticity and failure mode of nonlinear analysis. For the convenience of observation, deformation was amplified for 240 times. Fig. 23 depicts Von–Mises distribution and deformation under nonlinear critical loads, and Fig. 24 shows that the simulated deformation is similar to the text concave–convex phenomenon.

A numerical analysis considering residual stress was carried out, and it was found that the local buckling happened on one-quarter height from the top of column as shown in Fig. 24, which was consistent with the experimental results. The load-strain curves for typical locations from numerical analysis were shown in Fig. 25 (RS = residual stress), which were consistent with the experimental results. But, the

Table 3
Material properties in numerical simulation.

Dimension (mm)	Location	Yield strength (MPa)	Ultimate strength (MPa)	Elastic modulus (GPa)	Ultimate strain
□600 × 16	Side	350	450	210	0.1
	Corner	415	499		
□700 × 20	Side	340	443	210	0.1
	Corner	395	488		

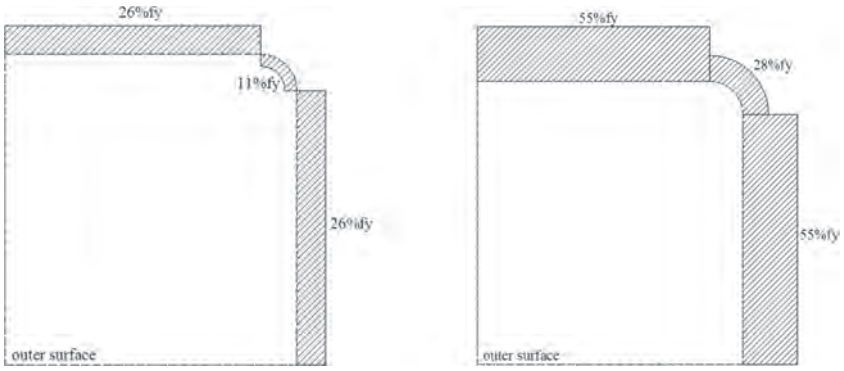

(a) Transverse cold-formed residual stress distribution on the external surface

(b) Longitudinal cold-formed residual stress distribution on the external surface

Fig. 21. Residual stress distribution model of cold-formed rectangular steel columns.

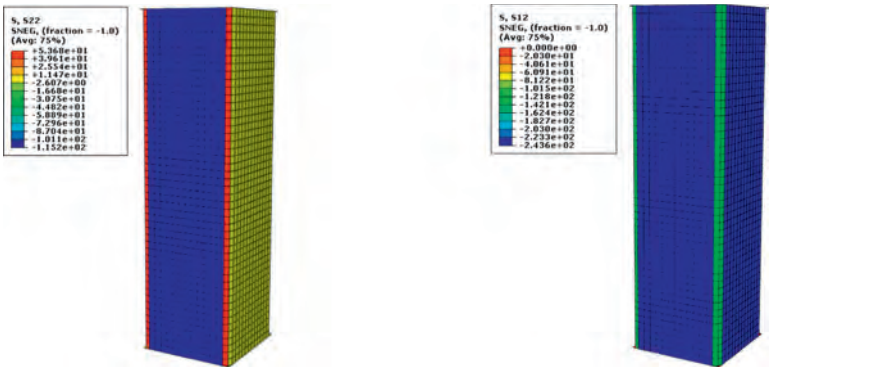

(a) Transverse cold-formed residual stress (b) Longitudinal cold-formed residual stress

Fig. 22. Stress distribution in the finite element model after the involvement of residual stress.

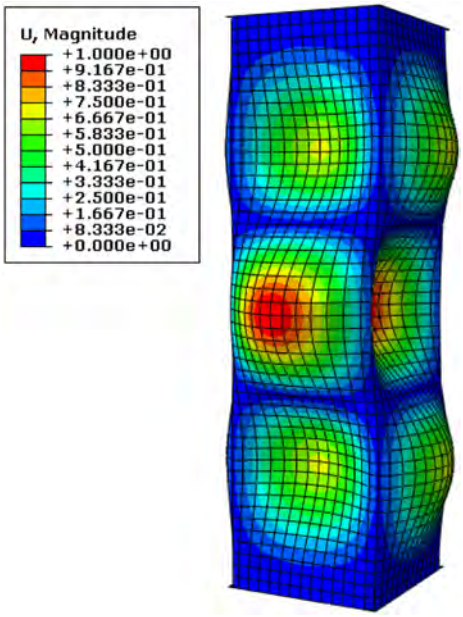

Fig. 23. First-order buckling analysis.

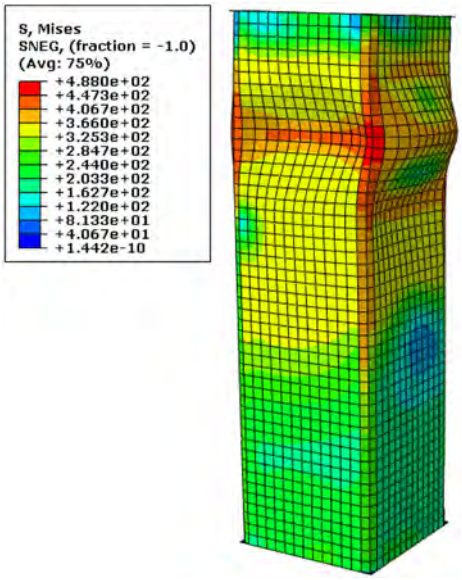

Fig. 24. Von Mises stress.

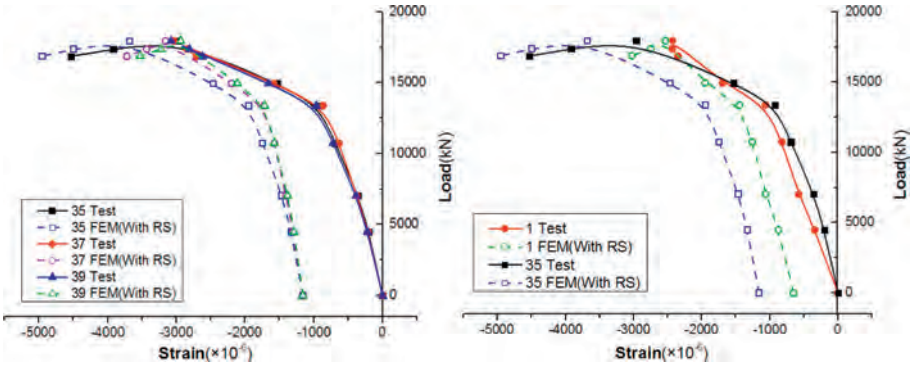

(a)measuring points on the 1/4, 1/2, 3/4 of buckling surface on flat location

(b) measuring points on the corner location & 1/4 of buckling surface on flat location

Fig. 25. Test and FEM (with residual stress) load–strain curves.

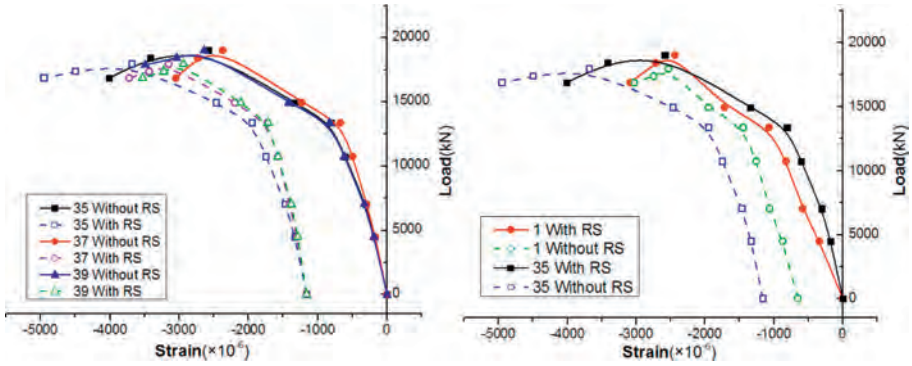

(a)measuring points on the 1/4, 1/2, 3/4 of buckling surface on flat location

(b) measuring points on the corner location& 1/4 of buckling surface on flat location

Fig. 26. FEM (with and without residual stress) load–strain curves.

initial strains from numerical analysis were larger than that obtained from tests due to the initial residual stress.

In order to study the effect of the residual stress on the structural behavior, a numerical analysis was also conducted without residual stress. Compared with the result considering the residual stress, it was found that the ultimate capacity reduced by 6% due to residual stress as shown in Fig. 26.

There had a difference of 3% between test result and numerical results for ultimate bearing capacity as listed in Table 4; and load-displacement curves from numerical analysis were similar to that from tests, but the initial rigidity was larger as shown in Fig. 13. The difference could be explained as follows:1) the measuring deviation from the equipment; 2) the differences of initial imperfection between FEM model and specimen; 3) the gaps existing among the components (such as specimen, sensors, the loading plate and the ground).

Table 4
Comparison between the tested and finite element simulations of bearing capacity.

Dimension	Tested ultimate bearing capacity (kN)	Simulated ultimate bearing capacity (kN)	Error
600 × 16	12,550	12,487	0.50%
700 × 20	17,950	18,486	2.99%

4.2. Parameter analysis and calculation formula of axial bearing capacity

Cold-formed rectangular steel columns with thick walls frequently bear large loads. Cold-formed rectangular steel columns are generally shorter than 24 m. The models of section columns (section dimension = 800 × 22, 700 × 20, and 600 × 16) with different normalized slenderness from 2.4 m to 24 m were established and analyzed, which obtained the stable bearing capacities of specimens (Table 5). Table 5 shows that the ultimate bearing capacity of cold-formed rectangular steel columns with large and thick walls decreases dramatically with the increase of the normalized slenderness.

The numerical simulation results were compared with the calculated results of different standard formulas. The following conclusions were obtained: (1) The stability coefficient (ϕ_3) of the *Technical Code of Cold-formed Thin-wall Steel Structures* [32] is small when $\lambda_c \le 0.380$, which indicates that the *Technical Code of Cold-formed Thin-wall Steel Structures* is conservative. (2) When $0.380 < \lambda_c \le 0.506$, the axial stability coefficient (ϕ_1) calculated by the model is small, which indicates that the axial stability coefficient calculated by the model is highly conservative. (3) When$0.506 < \lambda_c \le 1.266$, the axial stability coefficient (ϕ_4)

Table 5
Comparison between the numerical simulation results and calculated results of axial compression stability coefficient of cold-formed rectangular steel columns with thick walls.

Dimension (mm)	H (m)	λ_c	N_1 (kN)	ϕ_1	ϕ_2	ϕ_3	ϕ_4	ϕ_5	ϕ_1/ϕ_2	ϕ_1/ϕ_3
800 × 22	2.4	0.095	22,475	0.983	0.995	0.980	1.000	0.996	0.987	1.003
800 × 22	4.8	0.190	22,009	0.962	0.983	0.960	1.000	0.985	0.979	1.003
800 × 22	7.2	0.285	21,568	0.943	0.961	0.939	0.969	0.967	0.981	1.004
800 × 22	9.6	0.380	20,897	0.914	0.935	0.917	0.934	0.941	0.977	0.996
800 × 22	12.0	0.476	20,292	0.887	0.907	0.894	0.894	0.910	0.978	0.993
800 × 22	14.4	0.571	19,662	0.860	0.877	0.867	0.851	0.873	0.981	0.992
800 × 22	18.0	0.713	18,581	0.812	0.825	0.830	0.776	0.808	0.985	0.979
800 × 22	21.0	0.832	17,357	0.759	0.773	0.792	0.704	0.748	0.981	0.958
800 × 22	24.0	0.951	15,988	0.699	0.716	0.746	0.628	0.685	0.976	0.937
700 × 20	2.4	0.109	18,486	0.980	0.994	0.977	1.000	0.995	0.986	1.003
700 × 20	4.8	0.217	18,109	0.960	0.977	0.954	0.994	0.980	0.983	1.007
700 × 20	7.2	0.326	17,586	0.933	0.950	0.930	0.954	0.956	0.982	1.003
700 × 20	9.6	0.435	16,995	0.901	0.920	0.904	0.912	0.924	0.980	0.997
700 × 20	12.0	0.543	16,369	0.868	0.886	0.874	0.864	0.884	0.980	0.993
700 × 20	14.4	0.679	15,581	0.826	0.838	0.839	0.795	0.824	0.986	0.985
700 × 20	18.0	0.815	14,519	0.770	0.781	0.798	0.715	0.757	0.986	0.965
700 × 20	21.0	0.951	13,112	0.695	0.716	0.746	0.628	0.685	0.971	0.932
700 × 20	24.0	1.087	11,831	0.627	0.645	0.684	0.543	0.610	0.973	0.918
600 × 16	2.4	0.127	12,487	0.970	0.992	0.974	1.000	0.993	0.978	0.997
600 × 16	4.8	0.253	12,225	0.950	0.970	0.947	0.981	0.974	0.980	1.004
600 × 16	7.2	0.380	11,816	0.918	0.935	0.917	0.934	0.941	0.982	1.001
600 × 16	9.6	0.506	11,354	0.882	0.898	0.885	0.881	0.898	0.983	0.997
600 × 16	12.0	0.633	10,861	0.844	0.855	0.851	0.820	0.846	0.987	0.992
600 × 16	14.4	0.759	10,170	0.790	0.805	0.817	0.749	0.786	0.982	0.968
600 × 16	18.0	0.949	9019	0.701	0.717	0.747	0.630	0.686	0.977	0.938
600 × 16	21.0	1.108	7929	0.616	0.635	0.673	0.531	0.598	0.971	0.916
600 × 16	24.0	1.266	6883	0.535	0.551	0.583	0.444	0.511	0.970	0.917

Note: H is the height of steel column. λ_c is the normalized slenderness. N_1 is the axial compression ultimate bearing capacity of numerical simulation.ϕ_1 is axial compression stability coefficient, which is calculated by the model. ϕ_2 is the axial compression stability coefficient of the *Code for Design of Steel Structures* (GB 50017-2003) [36]. ϕ_3 is the stability coefficient of the *Technical Code of Cold-formed Thin-wall Steel Structures* [32]. ϕ_4 is the axial compression stability coefficient of the *European Design of Steel Structures* [35], and ϕ_5 is the axial compression stability coefficient of the *Australia/New Zealand Cold-formed Steel Structure* [34].

calculated by the *European Design of Steel Structures* [35] is small, which indicates that the *European Design of Steel Structures* is highly conservative.

According to ultimate bearing capacity (N_1), which is obtained from numerical analysis, the stability coefficient (ϕ_1) is calculated from Eq. (5). Figs. 27–30 present the variations of ϕ_1 normalized slenderness. Given that Eq. (5) does not involve the local buckling effects of steel plates in rectangular steel columns on ultimate bearing capacities, the buckling adjustment factor of plates is introduced to increase the calculation accuracy of the formula. The buckling adjustment factor of plates can be determined according to data statistics of ϕ_1/ϕ_2 in Table 5. The mean ϕ_1/ϕ_2 in Table 5 is 0.98, and the coefficient of variation is 0.00499. Therefore, the buckling adjustment factor of plates is $\beta_1 = 0.98$. Eq. (6) shows the corrected calculation formula of the stable bearing capacity of cold-formed rectangular steel columns with thick walls.

$$\frac{N}{\phi A_e} \le f, \tag{5}$$

$$\frac{N}{\phi A_e} \le \beta_1 f, \tag{6}$$

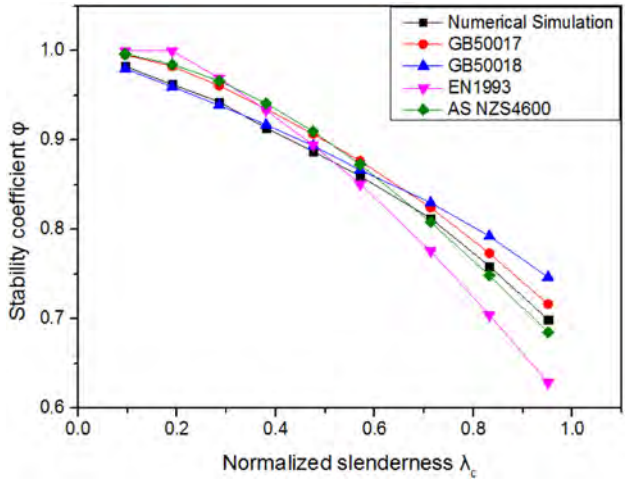

Fig. 27. 800 × 22 axial compression stability coefficient.

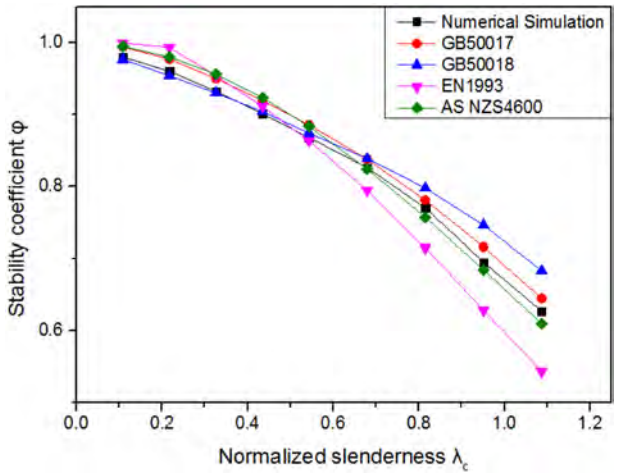

Fig. 28. 700 × 20 axial compression stability coefficient.

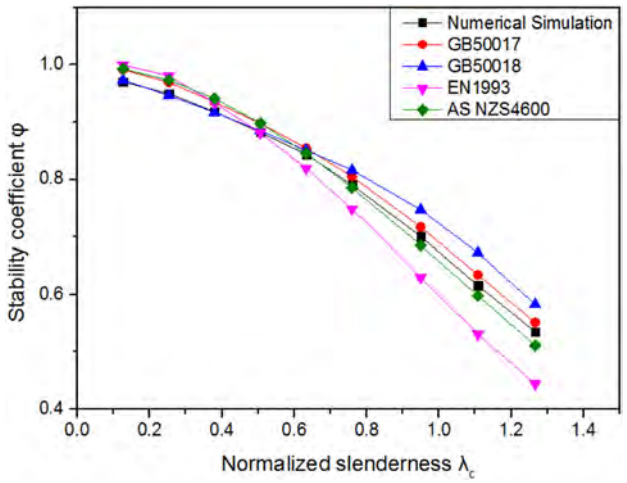

Fig. 29. 600 × 16 axial compression stability coefficient.

where f is the design strength of steel material, A_e is effective sectional area, and ϕ is axial compression stability coefficient of the steel structure.

4.3. Simulation of eccentric bearing capacity

In this study, the eccentric bearing capacity of cold-formed rectangular steel columns with large and thick columns has been discussed by using the finite element model (Fig. 31). Fig. 32 depicts the overall buckling failure mode of an 800 × 22 × 14,400 steel column when eccentricity is 0.667, and Fig. 33 illustrates the load–displacement curves under different eccentric distances. The ultimate bearing capacity of the same specimen declines dramatically with the increase of the eccentricity ratio. The two specimens show a nonlinear relationship. The midspan lateral displacement at ultimate bearing capacity increases with the increase of eccentricity. The higher the eccentricity is, the larger the early deformation and the smaller the axial rigidity will be. The deflections near the peak value are stable, and the ductility is good.

The finite element models of three dimensions (800 mm × 22 mm, 700 mm × 20 mm, and 600 mm × 16 mm) under different normalized

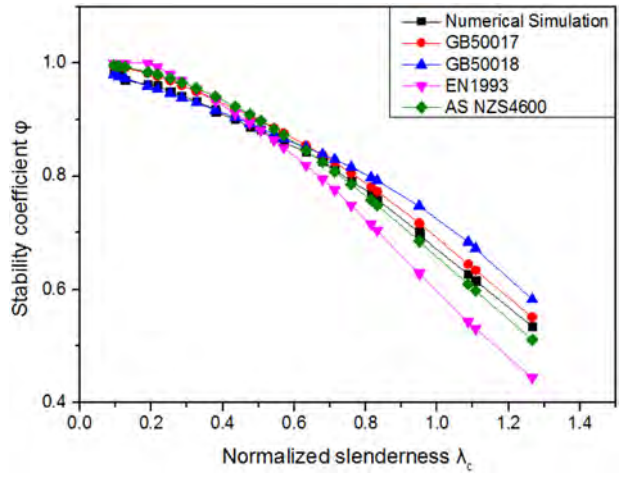

Fig. 30. Overall axial compression stability coefficient.

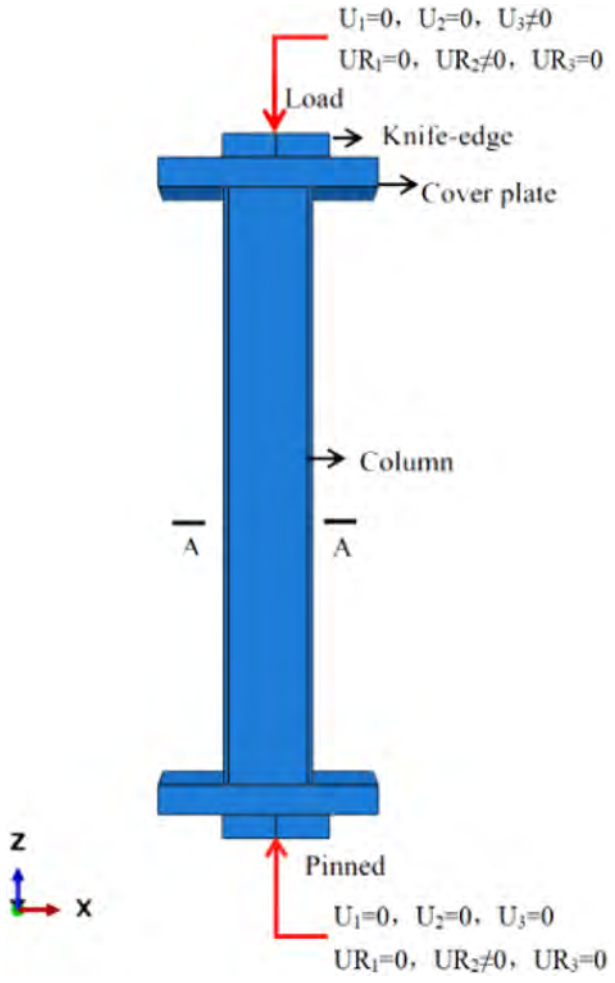

Fig. 31. Overall finite element model of eccentric bearing capacity.

slenderness and eccentric distances are established. Table 6 shows the bearing capacities of numerical simulation. The relation curves between the stable bearing capacity of cold-formed rectangular steel columns and different parameters are drawn on the basis of data in Table 6 (Fig. 34).

From Fig. 34, the ultimate bearing capacity of specimens decreases nonlinearly with the increase of normalized slenderness with a certain eccentricity. The ultimate bearing capacities decrease by 45.81%, 44.98%, and 42.78% when the eccentricities are 0, 0.333, 0.666, and 1 and the normalized slenderness (λ_c) increases from 0.127 to 1.266. Therefore, the ultimate bearing capacity of specimen decreases with the increase of an eccentric distance under fixed λ_c. The reduction amplitude declines gradually, and the ductility of specimens increases.

To sum up, the normalized slenderness and eccentricity are the main influencing factors of bearing capacity for cold-formed rectangular steel columns with large and thick walls. The bearing capacity of specimen decreases with the increase of the normalized slenderness or eccentricity. A nonlinear negative correlation is found between eccentricity and bearing capacity. Cold-formed rectangular steel columns with large and thick walls have good deformation performance. The ductility of specimens is positively related with normalized slenderness and eccentricity.

The calculation formula for the bearing capacity of cold-formed rectangular steel columns in the *Technical Code of Cold-*

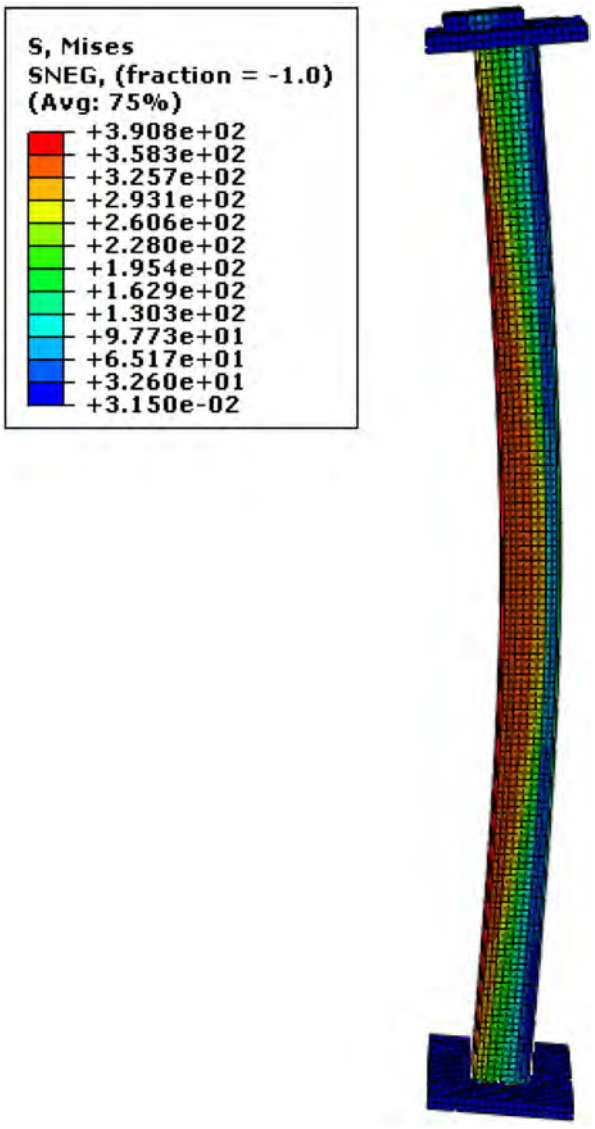

Fig. 32. Von–Mises stress.

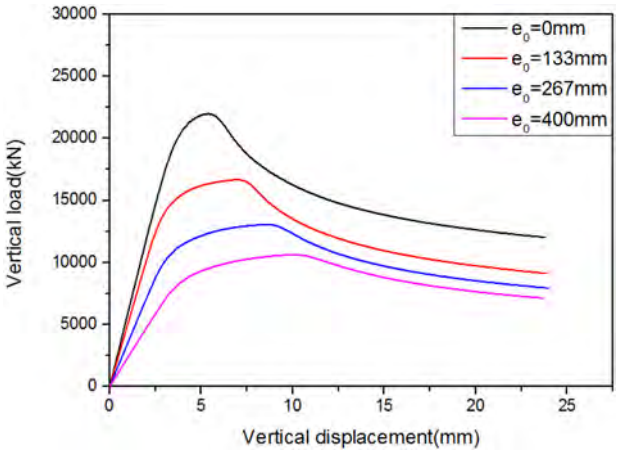

Fig. 33. Load–displacement curves of cold-formed steel columns under different eccentricity ratios.

Formed Thin-Walled Steel Structures [32] did not consider local plate buckling, and the local buckling adjustment factor of plates was used to increase calculation accuracy. According to numerical statistics of N_1/N_3 in Table 7, the value of N_1/N_3 decreases with the increase of normalized slenderness of the specimen, and the effect of the local buckling of the plates decreases with the increase of normalized slenderness of the column. The mean of N_1/N_3 in Table 7 is 1.11, the coefficient of variation is 0.056, and the maximum is 1.24. Therefore, a conservative plate local buckling adjustment factor can be determined. The local buckling adjustment factor of plates is $\beta_2 = 1.24$. In this study, the ultimate eccentric bearing capacity of cold-formed rectangular steel columns with thick walls should be calculated by Eq. (7):

$$\frac{N}{\beta_2 \phi A_e} + \frac{\beta_m M}{\left(1 - \frac{N}{\beta_2 N_E'}\phi\right) W_e} \le f \tag{7}$$

5. Conclusions

On the basis of the experimental study and numerical simulation analysis of the bearing capacity of cold-formed rectangular steel columns with thick walls under axial and eccentric compression loads, the conclusions are summarized as follows:

(1) For indirect cold-formed rectangular steel columns, the yield strength is 16%–19%, and the ultimate strength of the corner location is 8%–11%, which are higher compared with those of the side location, when the section dimension is 600–800 mm and the thickness ranges between 16 mm and 22 mm. The cold-formed effect of indirect cold-formed rectangular steel columns is lower than that of direct ones. The calculated results of yield strength formula that considered the cold-formed effect in *North America/Australia/New Zealand Design Specifications for Cold-formed Steel Structure* are close to test results. The calculated results are applicable to the yield strength of cold-formed rectangular steel columns with thickness over 16 mm.

(2) Local buckling of plates is the main axial compressive failure mode of cold-formed rectangular steel columns with thick walls. The stability coefficients of 2.4 m high steel columns with the section dimensions of 700 mm × 20 mm and 600 mm × 16 mm are 0.979 and 0.949, respectively, which indicates their good local stability.

(3) According to the test and numerical simulation data, the local bucking coefficient is introduced in the standard formula. Given the effects of the local buckling of plates on ultimate bearing capacity, the calculation formulas of ultimate axial compressive bearing and ultimate eccentric bearing capacities of cold-formed rectangular steel columns with large and thick walls are proposed. The calculated results conformed to the test and numerical simulation results.

Acknowledgments

This work was supported by the China Postdoctoral Science Foundation Funded Project (No. 2016M600188).

Table 6
Comparison between the numerical simulation results and calculated results of ultimate eccentric bearing capacity of cold-formed rectangular steel columns.

Dimension (mm)	H (m)	$N_{1e0.333}$ (kN)	$N_{1e0.667}$ (kN)	$N_{1e1.000}$ (kN)	$N_{2e0.333}$ (kN)	$N_{2e0.667}$ (kN)	$N_{2e1.000}$ (kN)	$N_{3e0.333}$ (kN)	$N_{3e0.667}$ (kN)	$N_{3e1.000}$ (kN)
800 × 22	2.4	16,900	13,060	10,910	16,106	12,067	9655	15,672	11,676	9312
800 × 22	4.8	16,512	12,730	10,714	15,879	11,913	9547	15,356	11,472	9172
800 × 22	7.2	16,071	12,410	10,498	15,498	11,658	9367	14,976	11,216	8991
800 × 22	9.6	15,491	12,014	10,058	15,024	11,337	9139	14,538	10,916	8778
800 × 22	12.0	14,877	11,466	9667	14,483	10,966	8874	14,043	10,576	8534
800 × 22	14.4	14,230	11,000	9290	13,885	10,555	8577	13,492	10,200	8264
800 × 22	18.0	13,249	10,186	8616	12,875	9863	8075	12,667	9632	7853
800 × 22	21.0	12,174	9436	8028	11,941	9226	7611	11,929	9133	7492
800 × 22	24.0	11,135	8805	7423	10,966	8561	7122	11,173	8628	7126
700 × 20	2.4	14,029	10,864	9004	12,790	9580	7665	12,430	9261	7387
700 × 20	4.8	13,601	10,580	8773	12,551	9420	7552	12,131	9066	7251
700 × 20	7.2	12,995	10,109	8440	12,169	9163	7371	11,767	8819	7077
700 × 20	9.6	12,385	9617	7996	11,711	8850	7147	11,341	8527	6868
700 × 20	12.0	11,764	9153	7622	11,185	8489	6888	10,854	8194	6630
700 × 20	14.4	10,865	8461	7036	10,439	7978	6518	10,231	7766	6320
700 × 20	18.0	9970	7773	6464	9604	7408	6104	9568	7316	5995
700 × 20	21.0	9017	7092	5916	8718	6804	5660	8883	6858	5663
700 × 20	24.0	8101	6429	5412	7819	6188	5202	8210	6411	5338
600 × 16	2.4	9478	7421	6063	8424	6316	5056	8181	6102	4871
600 × 16	4.8	9186	7213	5902	8218	6178	4959	7941	5944	4761
600 × 16	7.2	8805	6949	5731	7899	5962	4807	7644	5742	4617
600 × 16	9.6	8218	6460	5331	7525	5706	4623	7298	5505	4447
600 × 16	12.0	7677	6060	5006	7089	5408	4408	6923	5247	4262
600 × 16	14.4	7143	5627	4655	6604	5076	4167	6536	4982	4070
600 × 16	18.0	6289	4986	4147	5807	4532	3768	5914	4565	3768
600 × 16	21.0	5740	4464	3742	5125	4063	3420	5398	4223	3519
600 × 16	24.0	5136	4083	3469	4479	3612	3077	4892	3889	3275

Note: $N_{1e0.333}$, $N_{1e0.667}$, and $N_{1e1.000}$ are the ultimate bearing capacities gained from the numerical simulation when the eccentricities are 0.333, 0.667, and 1.000, respectively. $N_{2e0.333}$, $N_{2e0.667}$, and $N_{2e1.000}$ are the ultimate bearing capacities gained from the *Code for Design of Steel Structures* [36] when the eccentricities are 0.333, 0.667, and 1.000, respectively. $N_{3e0.333}$, $N_{3e0.667}$, and $N_{3e1.000}$ are the ultimate bearing capacities gained from the *Technical Code of Cold-formed Thin-wall Steel Structures* [32] when the eccentricities are 0.333, 0.667, and 1.000, respectively.

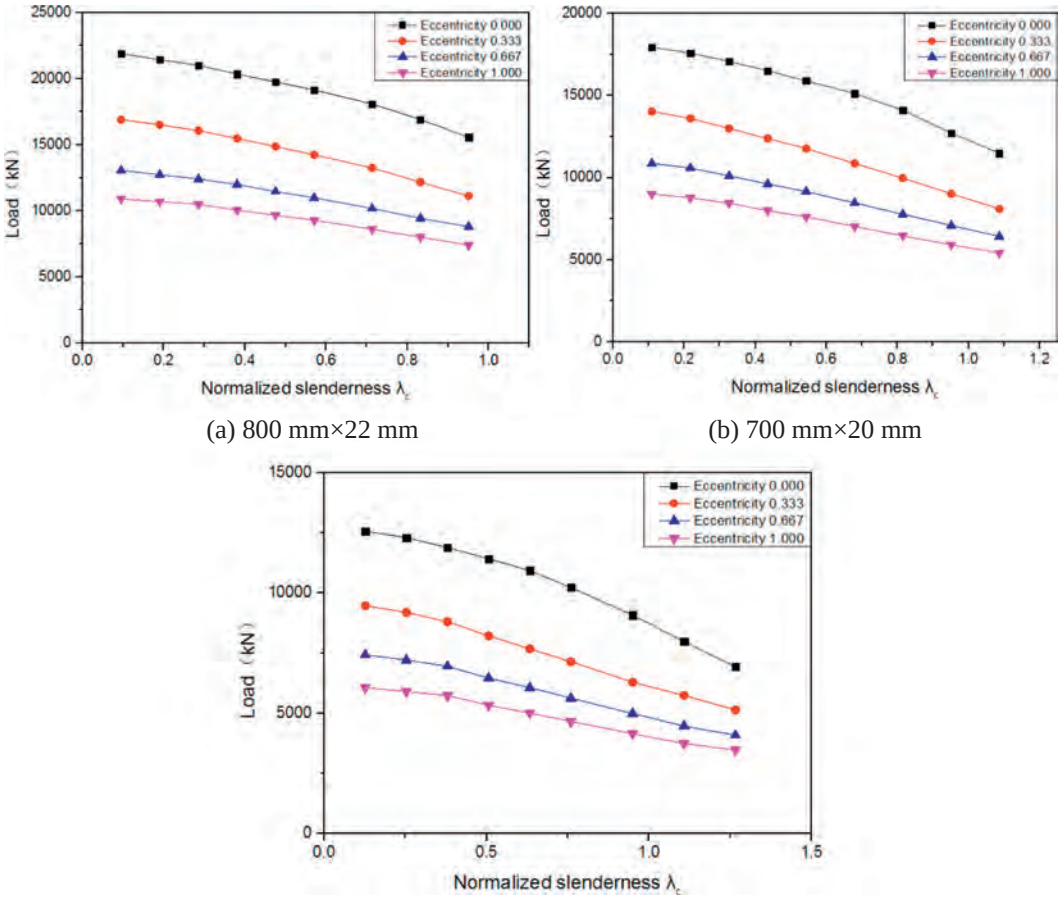

Fig. 34. Relation curves between the ultimate eccentric bearing capacity and normalized slenderness of cold-formed rectangular steel columns.

Table 7
Comparison between the numerical simulation results and calculated results.

Dimensions (mm)	H (m)	λ_c	$N_{1e0.333}/N_{2e0.333}$ (kN)	$N_{1e0.667}/N_{2e0.667}$ (kN)	$N_{1e1.000}/N_{2e1.000}$ (kN)	$N_{1e0.333}/N_{3e0.333}$ (kN)	$N_{1e0.667}/N_{3e0.667}$ (kN)	$N_{1e1.000}/N_{3e1.000}$ (kN)
800 × 22	2.4	0.095	1.05	1.08	1.13	1.08	1.12	1.17
800 × 22	4.8	0.190	1.04	1.07	1.12	1.08	1.11	1.17
800 × 22	7.2	0.285	1.04	1.06	1.12	1.07	1.11	1.17
800 × 22	9.6	0.380	1.03	1.06	1.10	1.07	1.10	1.15
800 × 22	12.0	0.476	1.03	1.05	1.09	1.06	1.08	1.13
800 × 22	14.4	0.571	1.02	1.04	1.08	1.05	1.08	1.12
800 × 22	18.0	0.713	1.03	1.03	1.07	1.05	1.06	1.10
800 × 22	21.0	0.832	1.02	1.02	1.05	1.02	1.03	1.07
800 × 22	24.0	0.951	1.02	1.03	1.04	1.00	1.02	1.04
700 × 20	2.4	0.109	1.10	1.13	1.17	1.13	1.17	1.22
700 × 20	4.8	0.217	1.08	1.12	1.16	1.12	1.17	1.21
700 × 20	7.2	0.326	1.07	1.10	1.15	1.10	1.15	1.19
700 × 20	9.6	0.435	1.06	1.09	1.12	1.09	1.13	1.16
700 × 20	12.0	0.543	1.05	1.08	1.11	1.08	1.12	1.15
700 × 20	14.4	0.679	1.04	1.06	1.08	1.06	1.09	1.11
700 × 20	18.0	0.815	1.04	1.05	1.06	1.04	1.06	1.08
700 × 20	21.0	0.951	1.03	1.04	1.05	1.02	1.03	1.04
700 × 20	24.0	1.087	1.04	1.04	1.04	0.99	1.00	1.01
600 × 16	2.4	0.127	1.13	1.18	1.20	1.16	1.22	1.24
600 × 16	4.8	0.253	1.12	1.17	1.19	1.16	1.21	1.24
600 × 16	7.2	0.380	1.11	1.17	1.19	1.15	1.21	1.24
600 × 16	9.6	0.506	1.09	1.13	1.15	1.13	1.17	1.20
600 × 16	12.0	0.633	1.08	1.12	1.14	1.11	1.15	1.17
600 × 16	14.4	0.759	1.08	1.11	1.12	1.09	1.13	1.14
600 × 16	18.0	0.949	1.08	1.10	1.10	1.06	1.09	1.10
600 × 16	21.0	1.108	1.12	1.10	1.09	1.06	1.06	1.06
600 × 16	24.0	1.266	1.15	1.13	1.13	1.05	1.05	1.06

References

[1] W.L. Xu, Z. Qian, Development and application of architectural roll formed shape in China, J. New Build. Mater. 8 (2005) 69–71 (in Chinese).
[2] L. Gardner, N. Saari, F. Wang, Comparative experimental study of hot-rolled and cold-formed rectangular hollow sections, Thin-Walled Struct. 48 (2010) 495–507.
[3] W.W. Yu, Cold-formed Steel Design, 3rd ed. John Wiley and Sons, New York, 2000.
[4] G.J. Hancock, Design of Cold-formed Steel Structures, 3rd ed. Australian Institute of Steel Construction, Sydney, 1998.
[5] Y. Ben, Y.H. Liu, Experimental investigation of cold-formed stainless steel columns, J. Struct. Eng. ASCE 129 (2) (2003) 169–176.
[6] T.M. Chan, X.L. Zhao, Y. Ben, Cross-section classification for cold-formed and built-up high strength carbon and stainless steel tubes under compression, J. Constr. Steel Res. 106 (2015) 289–295.
[7] O. Zhao, G. Leroy, Y. Ben, Structural performance of stainless steel circular hollow sections under combined axial load and bending-part 1: experiments and numerical modeling, Thin-Walled Struct. 101 (2016) 231–239.
[8] D.H. Wen, Z.Y. Shen, Y.Q. Li, et al., Experimental research on cold-formed thick-walled steel box stubs and comparison of results with related codes, J. Tongji Univ. 44 (8) (2016) 1190–1198 (in Chinese).
[9] M. Ashraf, L. Gardner, D.A. Nethercot, Strength enhancement of the corner regions of stainless steel cross-sections, J. Constr. Steel Res. 61 (1) (2005) 37–52.
[10] Y.Q. Li, G.W. Li, Z.Y. Shen, et al., Modification method for yield strength of cold-formed thick-walled steel sections considering cold-forming effect, J. Build. Struct. 36 (5) (2015) 1–7 (in Chinese).
[11] L.M. Li, X.L. Jiang, Z.H. Chen, et al., Strain hardening of thick-walled cold formed steel tube, J. Tianjin Univ. 41 (1) (2008) 85–91 (in Chinese).
[12] J. Chen, Study of Ultimate Axial Compressive Capacity of Cold-formed Medium Wall Square and Rectangular Hollow Steel Columns With Initial Imperfections, D. WuHan University of Technology, 2008.
[13] D.Y. Liu, H.B. Liu, Z.H. Chen, et al., Structural behavior of extreme thick-walled cold-formed square steel columns, J. Constr. Steel Res. 128((2017) 371–379.
[14] Tekcham Gishan Singh, Konjengbam Darunkumar Singh, Structural performance of YSt-310 cold-formed tubular steel stub columns, Thin-Walled Struct. 121 (2017) 25–40.
[15] J. Wang, S. Afshan, N. Schillo, et al., Material properties and compressive local buckling response of high strength steel square and rectangular hollow sections, Eng. Struct. 130 (2017) 297–315.
[16] A.Z. Zhu, Y.J. Guo, Experimental study on effect of cold-formed procedures to cold-formed steel members, J. Build. Struct. 35 (2) (2005) 40–47 (in Chinese).
[17] L.W. Tong, G. Hou, Y.Y. Chen, et al., Experimental investigation on longitudinal residual stresses for cold-formed thick-walled square hollow sections, J. Constr. Steel Res. 73 (2012) 105–116.
[18] X.Z. Zhang, S. Liu, M.S. Zhao, et al., Residual stress of cold-formed thick-walled steel rectangular hollow sections, J. Steel Compos. Struct. 22 (4) (2016) 837–853.
[19] A.Z. Zhu, Experimental Investigation of Cold-formed Effect on Thick-walled Steel Members and Analysis of Cold-formed Residual Stress Field, D. WuHan University, 2004.
[20] Y.J. Guo, A.Z. Zhu, Y.L. Pi, et al., Experimental study on compressive strengths of thick-walled cold-formed sections, J. Constr. Steel Res. 63 (2007) 718–723.
[21] John T. DeWolf, Peokoz Teoman, George Winter, Local and Overall Buckling of Cold-formed Members, ASCE, 1974 100.
[22] Y.P. Chu, Y. Yao, Y.J. Deng, et al., Research om behavior of cold-formed thin-walled long square steel tube columns under concentrically and eccentrically compressive loads, J. Build. Struct. 43 (21) (2013) 18–22 (in Chinese).
[23] A.Z. Zhu, H.P. Zhu, X.W. Zhang, et al., Experimental study and analysis of inner-stiffened cold-formed SHS steel stub columns, Thin-Walled Struct. 107 (2016) 28–38.
[24] J. Rondal, R. Maquoi, Stub-column strength of thin-walled square and rectangular hollow sections, Thin-Walled Struct. 3 (1985) 15–34.
[25] P.W. Key, G.J. Hancock, A theoretical investigation of the column behavior of cold-formed square hollow sections, Thin-Walled Struct. 16 (1993) 31–64.
[26] S. Ktitpornchai, F.G.A. Al-Bermani, S.L. Chan, Geometric and material nonlinear analysis of structures comprising rectangular hollow sections, Eng. Struct. 10 (1988) 13–23.
[27] Y.L. Pi, N.S. Trahair, Lateral buckling strengths of cold-formed rectangular hollow sections, Thin-Walled Struct. 16 (1995) 71–95.
[28] D. Dubina, V. Ungureanu, Effect of imperfections on numerical simulation of instability behavior of cold-formed steel members, Thin-Walled Struct. 40 (2002) 239–262.
[29] P.W. Key, G.J. Hancock, A theoretical investigation of the column behavior of cold-formed square hollow sections, Thin-Walled Struct. 16 (1993) 31–64.
[30] H. Wang, Study of Ultimate Axial Compressure of Cold-formed Medium Wall Hollow Sections With Initial Imperfections, D. Wuhan University of Technology, 2004.
[31] S. Min, A. Packer Jeffrey, Direct-formed and continuous-formed rectangular hollow sections – comparison of static properties, J. Constr. Steel Res. 92 (2014) 67–78.
[32] GB 50018-2002, Technical Code of Cold-formed Thin-walled Steel Structures, Standards Press of China, 2002 (in Chinese).
[33] AISI S100-2007, Specification for the Design of Cold-formed Steel Structural Members, Standards Press of North American, 2007.
[34] AS/NZS 4600-2005, Cold-formed Steel Structures, Standards Press of Australian and New Zealand, 2005.
[35] EN 1993-1-6-2006, Eurocode 3: Design of Steel Structures, Standards Press of Europe, 2006.
[36] GB 50017-2003, Code for Design of Steel Structures, Standards Press of China, 2003 (in Chinese).